



Cytology in cnidaria using *Exaiptasia* as a model

Thierry M. Work^{1,*}, Chutimon Singhakarn¹, Tina M. Weatherby²

¹US Geological Survey, National Wildlife Health Center, Honolulu Field Station, PO Box 50187, Honolulu, HI 96850, USA

²University of Hawaii at Manoa, Biological Electron Microscope Facility, Honolulu, HI 96822, USA

ABSTRACT: A need exists for additional methods to examine cnidaria at the cellular level to aid our understanding of health, anatomy, and physiology of this important group of organisms. This need is particularly acute given that disease is emerging as a major factor in declines of ecologically important functional groups such as corals. Here we describe a simple method to process cnidarian cells for microscopic examination using the model organism *Exaiptasia*. We show that this organism has at least 18 cell types or structures that can be readily distinguished based on defined morphological features. Some of these cells can be related back to anatomic features of the animal both at the light microscope and ultrastructural level. The cnidome of *Exaiptasia* may be more complex than what is currently understood. Moreover, cnidarian cells, including some types of cnidocytes, phagocytize cells other than endosymbionts. Finally, our findings shed light on morphologic complexity of cell-associated microbial aggregates and their intimate intracellular associations. The tools described here could be useful for other cnidaria.

KEY WORDS: Cnidocytes · Nematocyst · Phagocytosis · Bacterial clusters · Clinical pathology

1. INTRODUCTION

Coral reefs harbor a rich biodiversity of fauna and flora but are facing unprecedented threats due to overfishing, climate change-induced bleaching events, land-based pollution, and most recently, disease outbreaks (Work 2023). A vivid illustration of the latter are the catastrophic mortalities of multiple species of corals throughout the Western Atlantic attributed to stony coral tissue loss disease (SCTLD) that have been ongoing since its discovery in Florida, USA, in 2014 (Precht et al. 2016). The cause of SCTLD remains unknown, although tissue loss lesions in corals from Florida are associated with pathology of endosymbionts (Landsberg et al. 2020) possibly caused by a virus (Work et al. 2021). Outside of Florida, it is unclear whether SCTLD has a single cause.

Significant efforts are ongoing to determine the cause of SCTLD; however, these are hampered by a

lack of understanding of host physiology and a dearth of tools to examine coral health. Tools commonly used to assess coral health include field surveys and transmission (Aeby et al. 2019), microbial culture or metagenomics (Ushijima et al. 2020), and various other '-omics' (Traylor-Knowles et al. 2022). The use of microscopy to characterize host cell pathology is a fundamental tool of wildlife health assessment (Work & Meteyer 2014), and histology is playing an increasingly important role in evaluating coral health (Hawthorn et al. 2023).

A useful complement to histology is cytology. Histology is a relatively complex process requiring embedding of tissues in resins or paraffin, thin sectioning onto slides, and staining; the technique allows for detailed examination of the cellular anatomy of host tissues (Al-Abbadi 2011). In contrast, cytology uses a simpler approach where tissues or cell suspensions are daubed or smeared, respectively, onto microscope

*Corresponding author: thierry_work@usgs.gov

slides and stained. Compared to histology, the focus of cytology is microscopic examination of individual cells rather than tissue architecture (Meinkoth & Cowell 2002). The use of cytology for diagnostics has some advantages over histology. For instance, procuring samples is less invasive, involving techniques such as blood draws or fine needle aspirates (Meinkoth & Cowell 2002). Cytology can also complement histology by offering views of single cells and morphologic changes that are sometimes not as visible in tissue sections. Whilst histology generally offers more diagnostic information, some diseases are more readily diagnosed by cytology. For example, trichomoniasis, a protozoal disease of birds, is more readily diagnosed by cytology, because the host inflammatory response often obscures visualization of causative trichomonads in tissue sections examined by histology (Arenales et al. 2014). Malaria is another disease commonly diagnosed by cytology because details of the intracellular parasites are most evident using this technique (Atkinson & Samuel 2010).

Cytology in cnidaria has a rich history. The seminal work of Hyman (1940) on cellular anatomy of cnidaria serves as a touchstone on the topic, whilst morphologic studies by Weill (1934) provided foundational knowledge of the stinging cells of cnidaria. David (1973) used acetic acid and glycerin to dissociate hydra cells, and more recently, Kirk & Xiang (2022) used enzymatic methods to dissociate cells from a single *Exaiptasia diaphana*. All of these studies used bright field microscopy of unstained cells to examine cell morphology. In contrast, veterinary cytology depends heavily on examination of cells stained with polychrome Romanowsky-type stains (Romanowsky 1890) that offer details on cytoplasmic and nuclear structures not readily visible on brightfield microscopy. Moreover, the use of acids and enzymes to dissociate cells could introduce artifacts that complicate interpretation of cytologic morphology. Thus, to date, the application of cytology as used in a clinical setting for veterinary medicine has not yet been applied to cnidaria. Here we tried to build upon existing methods to evaluate a simplified protocol to dissociate cells from a cnidarian, *E. pulchella*, widely considered to be a suitable model for this class of organisms (Weis et al. 2008). We then described cytologic morphology using commercially available Romanowsky-like stains and tried to localize cells at the tissue level using histology and at the ultrastructural level using electron microscopy. Our findings show at least 18 distinguishable cell types or structures in *E. pulchella* and a complex cnidome, and provide insights on potential developmental morphologies of certain cells.




















2. MATERIALS AND METHODS

2.1. Cytology

Six *Exaiptasia pulchella* were obtained from flow-through seawater tanks at the State of Hawaii coral nursery on Sand Island, Oahu, in March 2023. These animals were deemed apparently normal based on uniform coloration, prominent extended corona of tentacles, ability to adhere to sides of tanks, and rapid withdrawal when stimulated. Animals were held in the same seawater as flow-through tanks at room temperature for 1–5 h prior to processing. For cell dissociation, each animal underwent the following procedure: (1) animals were relaxed for 5–10 min in 5% magnesium chloride at room temperature (Martell et al. 2016) in calcium–magnesium-free seawater (CMFSW; 449 mM NaCl, 9 mM KCl, 33 mM Na₂SO₄, 2.15 mM NaHCO₃, 10 mM Tris-HCL pH 8, 2.5 mM EDTA pH 8); (2) each animal was then dissected with fine forceps and Pasteur pipettes into 5 compartments including tentacles, corona of tentacle bases, body, acontia, and internal mesenterial filaments, each of which was separately placed in 500–1000 µl CMFSW; (3) tissues were allowed to incubate at room temperature for 1–3 h; (4) tissues were then gently dissociated by pipetting up and down using a 1000 µl pipettor or Pasteur pipettes until the supernate became cloudy and brown (about 1–3 min). A 50 µl aliquot of cell suspension was then mixed with 50 µl of 10% formalin in seawater, and cells were concentrated onto a microscope slide using a syringe barrel apparatus clipped onto filter paper (Work et al. 2020). Slides were then air-dried, stained with HEMA 3 (Fisher Scientific) comprising a series of reagents including fixation in methanol (~10 s), followed by dipping slides for about 5 s in an acidic stain (Eosin Y), followed by about 5 s in a basic stain (methylene blue), then rinsing in tap water, air-drying, and examining under an oil-immersion lens. We examined fixed rather than fresh cells directly placed on slides, because pilot studies showed that fresh cells on slides were sparse and appeared smudged or indistinct, whereas cytoplasmic and nuclear details were far superior for fixed cells concentrated on the syringe barrel apparatus.

Cells or structures were grouped into 18 morphotypes (Table 1). Endosymbionts were characterized by presence of a pyrenoid and occasional cell division (Camaya 2020). Granule or pigment cells were those with intracytoplasmic eosinophilic or melanin-like granules, respectively (Hawthorn et al. 2023). Cnidocytes were classified as per Gundlach & Watson (2019). Cell-associated microbial aggregates

Table 1. *Exaiptasia pulchella* cell types and morphological features of cells from cytology

Cell type	Sub-type	Cell morphology	Example
Cnidocytes and discharged nematocysts	Nematocysts	Elongated and dark with no discernable internal structures; ca. 3–5 μm wide to 10–25 μm long (Fig. 1A,B)	
	Type 1 cnidocytes	Allantoid and basophilic with a laterally placed nucleus with larger examples having a central barb; ca. 5–10 μm wide by 30–70 μm long (Fig. 1C,D)	
	Type 2 cnidocytes	Elongate cells with a large eccentric nucleus containing an allantoid structure with a central barb ca. 10 μm wide by 30 μm long (Fig. 1E–G)	
	Type 3 cnidocytes	Small to large fabiform to allantoid cells with a deeply basophilic cytoplasm with ill-defined pink intracytoplasmic inclusions and a central filament; ca. 10–15 μm wide by 10–80 μm long (Fig. 1H–N)	
	Type 4 cnidocytes	Round cell with basophilic cytoplasm containing an atrichous eosinophilic-to- polychrome filament attached to a club-like structure; ca. 8–20 μm diameter (Fig. 2A–E)	
	Spirocytes	Round to ovoid cell with intracytoplasmic coiled bundle of eosinophilic filaments; ca. 10 \times 12 μm (Fig. 2F–J)	
Granule cells	Type 1 granule cells	Round to amorphous cells with a blue cytoplasm stippled with variable numbers of distinct fine dull eosinophilic granules; ca. 8–20 μm diameter (Fig. 3A–D)	
	Type 2 granule cells	Round to amorphous cell with sparse, large, distinct round eosinophilic cytoplasmic granules; ca. 12–20 μm diameter (Fig. 3E,F)	
	Type 3 granule cells	Round cells with a cytoplasm replete with coarse brick-red granules; ca. 8 μm diameter (Fig. 3G)	
	Type 4 granule cells	Round cells with a cytoplasm replete with distinct bright eosinophilic granules; ca. 5 μm diameter (Fig. 3H)	
	Type 5 granule cells	Round cells with a cytoplasm replete with basophilic granules; ca. 10 μm diameter (Fig. 3I)	
	Type 6 granule cells	Round cells with a foamy basophilic cytoplasm and sparse distinct coarse angular sided black-blue granules; ca. 10–12 μm diameter (Fig. 3J)	
Mucocytes	Small to large round cells with a cytoplasm obscured by coarse, somewhat distinct, pink-purple granules; ca. 12–40 μm diameter (Fig. 3K–O)		
Interstitial cells	Small to large round cells with a basophilic cytoplasm and an eccentric nucleus sometimes with a flagellum; ca. 5–15 μm diameter (Fig. 4A–E)		
Endosymbionts	Round cells with dark blue to brown-stippled cytoplasm with a pyrenoid; ca. 8–10 μm diameter (Fig. 4F–I)		
Mycocyte-like cells	Round to highly pleomorphic with appendages, homogeneous basophilic cytoplasm, and eccentric nucleus; ca. 10 μm diameter to 20 μm long (Fig. 4J–L)		
Pigment cells	Round cells with granular brown pigment in basophilic cytoplasm; ca. 15 μm diameter (Fig. 4M)		
Cell-in-cell interactions	Host cells enveloping and internalizing other cell types. Seen in Type 1 granule cells (Fig. 4N,O), type 4 cnidocytes (Fig. 4P), and interstitial cells (Fig. 4Q–S)		
Cell-associated microbial aggregates	Intra- or extracellular oblong clusters of tightly packed basophilic rods and a club-like structure. Extracellular clusters can become larger with dissociating bacterial cells; ca. 8–70 μm diameter (Fig. 5A–E)		

were described as per Work & Aeby (2014). Interstitial cells followed the terminology of David (1973). Cytology of mucocytes and myocyte-like cells has not been previously described, so we elevated those terms for purposes of this paper. For a given cell morphology, we inferred that smaller cells of similar morphology were younger stages of the larger cells, a reasonable conjecture given that eukaryotic cells grow in size with maturation (Amodio & Skotheim 2016). For each of 5 tissue compartments for 6 anemones, these cell types were enumerated for 20 oil-immersion microscope fields. Field of view (FOV) for all examinations calculated by field number of eyepiece (FN = 20)/objective magnification (100×) was 0.2

2.2. Histology and electron microscopy

For histology, 8 *E. pulchella* separate from those used for cytology were fixed whole in 10% formalin and seawater; tissues were processed and embedded in paraffin, and sections were stained with hematoxylin and eosin. For electron microscopy, sections of animals used for cytology were fixed in electron microscopy fixative (McDowell & Trump 1976) and processed for electron microscopy examination as described elsewhere (Work et al. 2021).

3. RESULTS

3.1. Cnidocytes and nematocysts

Six types of cnidocytes or nematocysts were seen. Discharged cnidae (Fig. 1A) or nematocyst capsules (Fig. 1B) were small (ca. 10 μm long) and dark with no discernable internal structures. Type 1 cnidocytes were elongated and blue, with larger examples having a central barb (Fig. 1C,D). Type 2 cnidocytes were cells with a large eccentric nucleus, a squatter appearance, and contained an allantoid structure with a central barb (Fig. 1E–G). Type 3 cnidocytes were the largest (exceeding 70 μm), with a deeply basophilic cytoplasm with ill-defined pink intracytoplasmic inclusions (Fig. 1H–N). Type 4 cnidocytes comprised a cell with basophilic cytoplasm containing an atrichous red filament attached to a club-like structure (Fig. 2A–E). Spirocytes adopted the typical appearance of tightly coiled bundle of red filaments (Fig. 2F–J). Discharged cnidae/nematocysts were common in all tissue compartments, whereas cnidocytes of Types 1 and 4 and spirocytes dominated in

tentacles, and Type 1 cnidocytes were common in acontia (Fig. A1 in the Appendix).

3.2. Granule cells

Six types of granule cells were seen. Type 1 granule cells were round to amorphous cells with a basophilic cytoplasm stippled with variable numbers of distinct fine dull eosinophilic granules and had an estimated size ranging from ca. 8 to 20 μm (Fig. 3A–D). Type 2 granule cells had sparse, large, distinct, round red cytoplasmic granules measuring ca. 12–20 μm (Fig. 3E,F). Type 3 granule cells were smaller (ca. 8 μm) and had a cytoplasm replete with coarse brick-red granules (Fig. 3G). Type 4 granule cells were the smallest type of granulocyte (ca. 5 μm) with a cytoplasm replete with distinct bright eosinophilic granules (Fig. 3H). Type 5 granule cells were ca. 10 μm and contained distinct intracytoplasmic basophilic granules (Fig. 3I). Type 6 granule cells were of similar size to Type 5 granule cells with a foamy basophilic cytoplasm and sparse, distinct, coarse, angular black-blue granules (Fig. 3J). Type 1 granule cells dominated in all tissue compartments (Fig. A2).

3.3. Other cells

Mucocytes had a broad size range (ca. 15–80 μm) and had a cytoplasm replete with coarse pink-purple granules that completely filled and obscured the cytoplasm, thereby distinguishing these cells from granulocytes (Figs. 3K–O). Interstitial cells (presumed epidermis, gastrodermis, or calicodermis) ranged in size from ca. 5 to 15 μm and comprised a blue cytoplasm with an eccentric nucleus (Fig. 4A–E). Endosymbionts were either *in hospite* (inside the cnidarian host cell) (Fig. 4F) or extracellular, had a pyrenoid, and sometimes golden-brown intracytoplasmic granules (Fig. 4G–I). Myocyte-like cells ranged from small and round (Fig. 4J), to large and oblong (Fig. 4K), to highly pleomorphic with appendages, eccentric nucleus, and a homogeneous deeply basophilic cytoplasm with distinct borders that distinguished them from other cell types (Fig. 4L). Pigment cells were ca. 15 μm and had granular brown pigment in blue cytoplasm (Fig. 4M). Cell-in-cell interactions were seen with 3 cell types including granule cells (Fig. 4N,O), Type 4 cnidocytes (Fig. 4P), and interstitial cells (Fig. 4Q–S), all engulfing or containing intracytoplasmic unidenti-

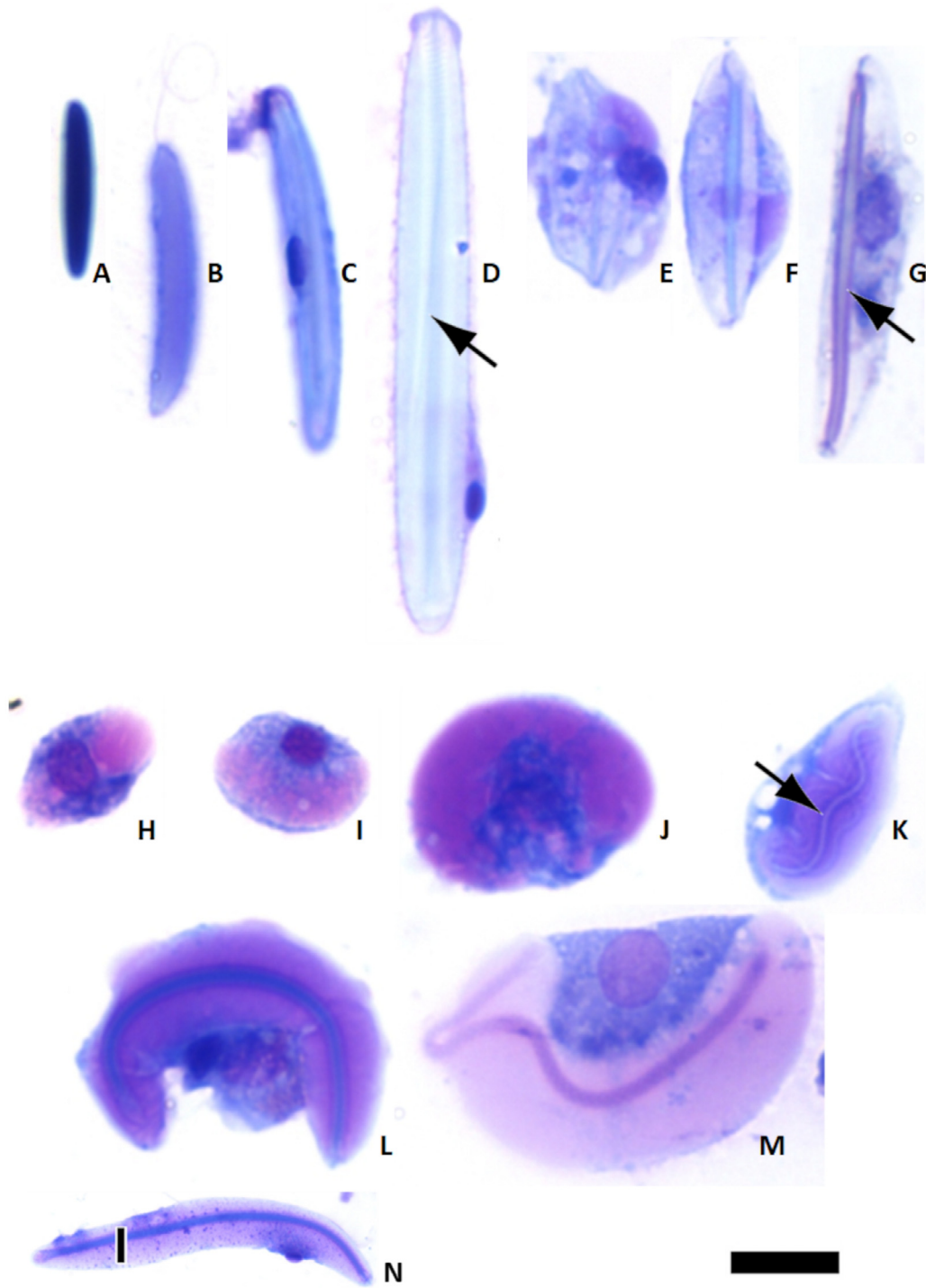


Fig. 1. Nematocysts, nematocyst capsules, and cnidocytes Types 1–4 in apparently healthy *Exaiptasia pulchella* stained with HEMA-3. All images scaled to bar on lower right except for (N) with superimposed vertical scale bar; both bars = 10 μm . (A) Nematocysts; note dense black small allantoid structure. (B) Discharged nematocyst capsules. (C,D) Type 1 cnidocyte; note variably sized allantoid to elongate basophilic structure with presumed immature (C) to more mature (D) exemplars having a central shaft (arrow) and eccentric host cell nucleus. (E–G) Type 2 cnidocyte with presumed immature (E), intermediate (F), and more mature cell (G) with allantoid intracytoplasmic structures containing a central shaft (arrow). (H–N) Type 3 cnidocyte; immature cell with nucleus nested in eosinophilic intracytoplasmic inclusion (H), different view of cell with eosinophilic inclusion wrapping around nucleus (I), enlargement of eosinophilic inclusion (J), formation of nematocyst filament within eosinophilic matrix (K), enlargement of nematocyst wrapping around nucleus (L), different version of similar cell (M), and large mature cell (N)

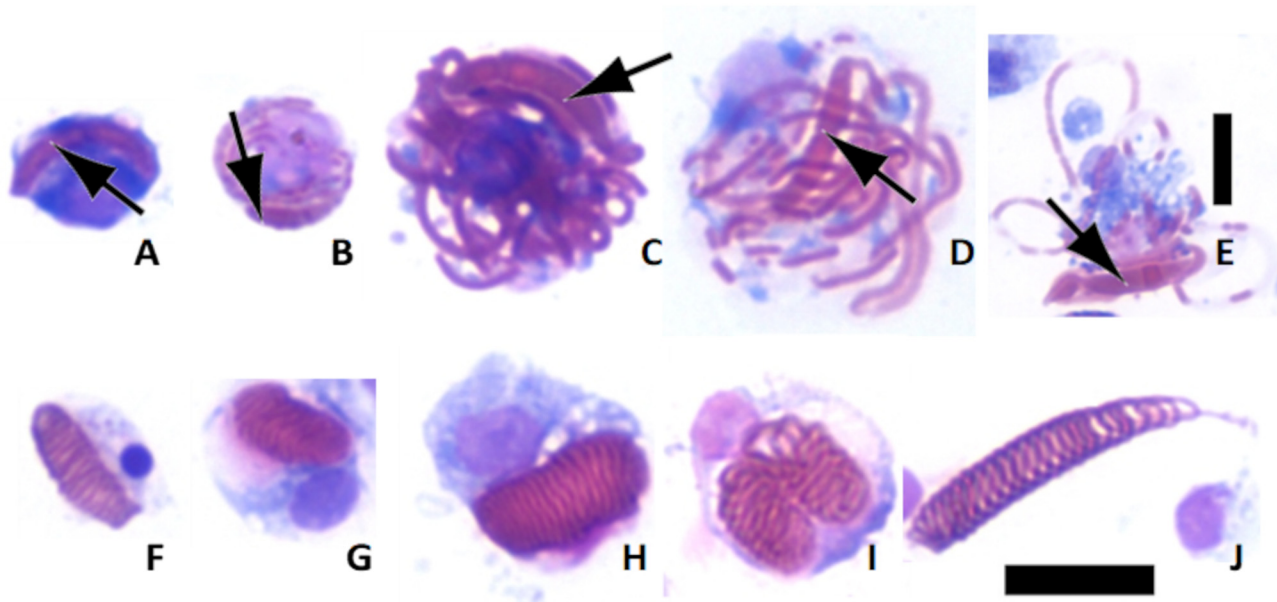


Fig. 2. Type 4 cnidocytes and spirocytes in apparently healthy *Exaiptasia pulchella* stained with HEMA-3. All images scaled to bar on lower right except for (E) with superimposed vertical scale bar; both bars = 10 μm . (A–E) Various exemplars of Type 4 cnidocytes. (A) Presumed early stage with intracytoplasmic eosinophilic club-like structure (arrow). (B) Formation of elongate eosinophilic intracytoplasmic filaments attached to club-like structure (arrow). (C) Larger, more substantial densely packed eosinophilic filament with club-like structure (arrow). (D) Larger cell with more loosely spaced filaments and club-like structure (arrow). (E) Discharged nematocyst comprising atrichous polychromatic filament and club-like structure (arrow). (F–J) Various exemplars of spirocytes. Presumed early-stage cell with coiled spirocyst and nucleus (F); immature cell with spirocyst and intracytoplasmic eosinophilic inclusion (G); more mature cell with larger, more loosely packed coiled filament (H); larger cell with coiled filament adopting a folded configuration (I); discharged spirocysts adjacent to separate interstitial cell at lower right (J)

fied cells. Interstitial cells and endosymbionts dominated in all tissue compartments aside from acontia, where endosymbionts were rare (Fig. A3).

3.4. Cell-associated microbial aggregates

Cell-associated microbial aggregates were either intra- or extracellular. Intracellular aggregates were tightly packed and attached to a club-like structure (Fig. 5A–C). Extracellular aggregates were similar but tended to become larger with dissociation of cells (Fig. 5D–F). Cell-associated microbial aggregates were not seen when formally quantified by cytology (Fig. A3).

3.5. Tissue-level identification

We could see 13 of 18 cell types identified on cytology in histology sections. Interstitial cells and mucocytes were seen in all tissue compartments (Fig. 6A), whereas endosymbionts were seen in all but mesenteries. Spirocytes and Type 4 cnidocytes were found

in tentacles (Fig. 6B), whereas Types 1 through 3 cnidocytes were in mesenterial filaments (Figs. 6C,D). Myocytes were in myonemes and mesoglea (Fig. 6E). Bacterial aggregates were seen only in tentacle epidermis (Fig. 6F). Cells not clearly seen on histology included pigment cells, Types 1, 2, 4, and 5 granule cells, and cell-in-cell interactions.

We could see 7 cell types on transmission electron microscopy (TEM) and putatively identified all granule cells. Nematocysts (cf. Fig. 1A,B, light microscopy [LM]) were small with a homogeneous matrix and thick capsule (Fig. 7A, TEM). Type 1 cnidocytes (Fig. 1C,D, LM) had a thick capsule enclosing a core of mixed electron density with an electron-dense filament surrounded by ornate trichae (Fig. 7B, TEM). Putative Type 3 cnidocytes (Fig. 1H–N, LM) had a large electron-dense matrix surrounded by a thick capsule (Fig. 7C, TEM). Type 4 cnidocytes (Fig. 4A–E, LM) had a cytoplasm occupied by a thick electron-dense filament with an ornate club structure (Fig. 7D, TEM). Spirocytes (Fig. 4F–J, LM) had an electron-lucent cavity containing peripherally arranged trichous filaments (Fig. 7E, TEM). Type 1 (Fig. 3A–D LM; Fig. 7F, TEM), Type 2 (Fig. 3E,F, LM; Fig. 7G,

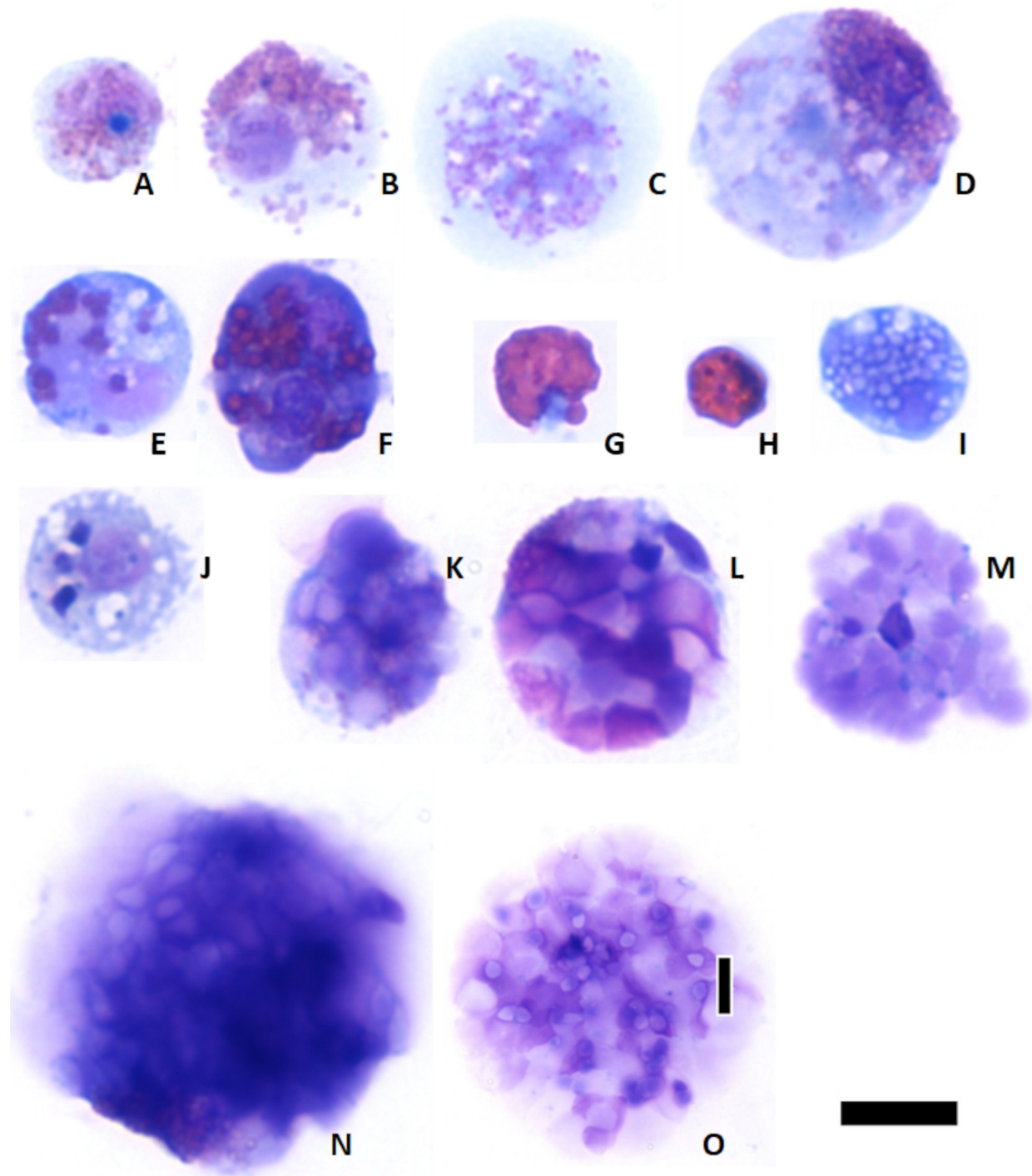


Fig. 3. Representative granule cells and mucocytes in apparently healthy *Exaiptasia pulchella* stained with HEMA-3. All images scaled to bar on lower right except for (O) with superimposed vertical scale bar; both bars = 10 μ m. (A) Small Type 1 granular cell with condensed nucleus. (B) Medium size Type 1 granular cell with pale blue cytoplasm and scattered red-purplish intracytoplasmic stippling. (C) Larger Type 1 granule cells. (D) Large Type 1 granule cells with intracytoplasmic granules clustered to one side. (E) Type 2 granule cell with coarse eosinophilic round granules within blue cytoplasm and eccentric nucleus. (F) Type 2 granule cell with more deeply basophilic cytoplasm and coarse granules. (G) Type 3 granule cell; note cytoplasm packed with densely packed brick-red granules and eccentric nucleus. (H) Type 4 granule cell; note small size relative to other cells and cytoplasm packed with bright eosinophilic granules. (I) Type 5 granule cell; note cytoplasm replete with blue-pink granules. (J) Type 6 granule cell; note basophilic foamy cytoplasm with sparse coarse dark basophilic intracytoplasmic granules. (K–O) Mucocyte; note 5 exemplars with cytoplasm replete with large ill-defined purple granules and wide range of sizes ranging from small (K) to very large (O)

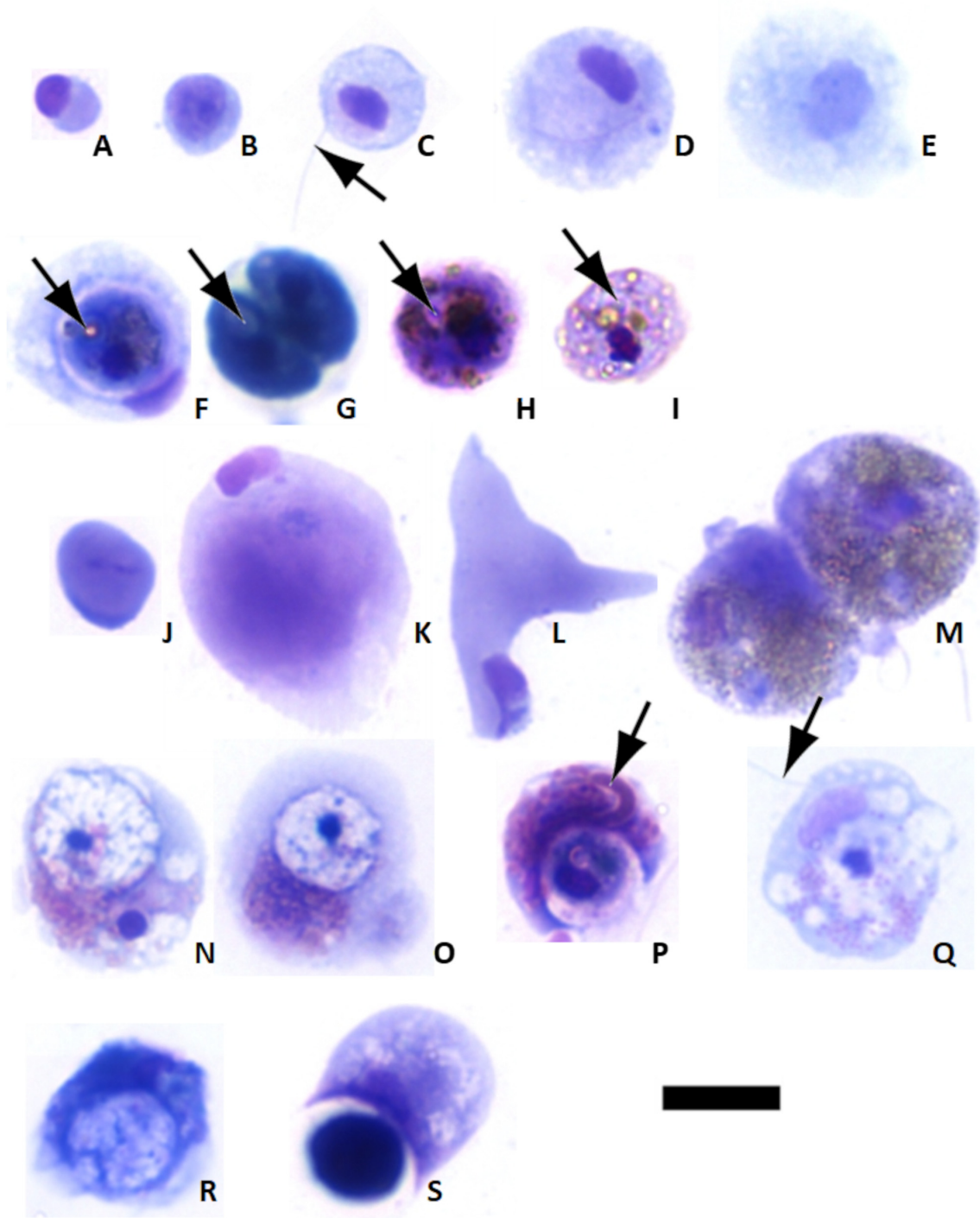


Fig. 4. Other cell types including (A–E) interstitial cells, (F–I) endosymbionts, (J–L) myocyte-like cells, (M) pigment cells, and (N–S) cell-in-cell interactions in apparently healthy *Exaiptasia pulchella* stained with HEMA-3. All images are relative to scale bar at lower right; bar = 10 μ m. (A) Small interstitial cell with eccentric condensed nucleus and pale basophilic cytoplasm. (B) Larger interstitial cell with large nucleus and pale blue cytoplasm. (C) Larger interstitial cell with flagellum (arrow). (D) Large interstitial cell with pale blue cytoplasm and faint pale intracytoplasmic inclusion. (E) Larger interstitial cell with pale foamy cytoplasm. (F) Endosymbiont *in hospite*; note eccentric host cell nucleus (bottom) and pyrenoid (arrow). (G) Dividing endosymbionts; note cleavage between 2 cells and pyrenoid (arrow). (H) Endosymbiont with pyrenoid (arrow), basophilic cytoplasm, and intracytoplasmic granules. (I) Endosymbiont with pale blue cytoplasm and brown granules and pyrenoid (arrow). (J) Small myocyte-like cell with deeply basophilic cytoplasm and eccentric nucleus. (K) Large myocyte-like cell with basophilic cytoplasm and eccentric nucleus. (L) Pleomorphic myocyte-like cell with angular appendages and eccentric nucleus. (M) Pigment cells containing intracytoplasmic brown granules. (N,O) Type 1 granule cells phagocytizing unidentified cell. (P) Type 4 cnidocyte enveloping unidentified cell; note intracytoplasmic eosinophilic filaments with club-like structure (arrow). (Q) Interstitial cell with flagellum (arrow) and foamy cytoplasm with intracytoplasmic unidentified cell. (R) Interstitial cell with intracytoplasmic unidentified cell. (S) Interstitial cell enveloping unidentified object

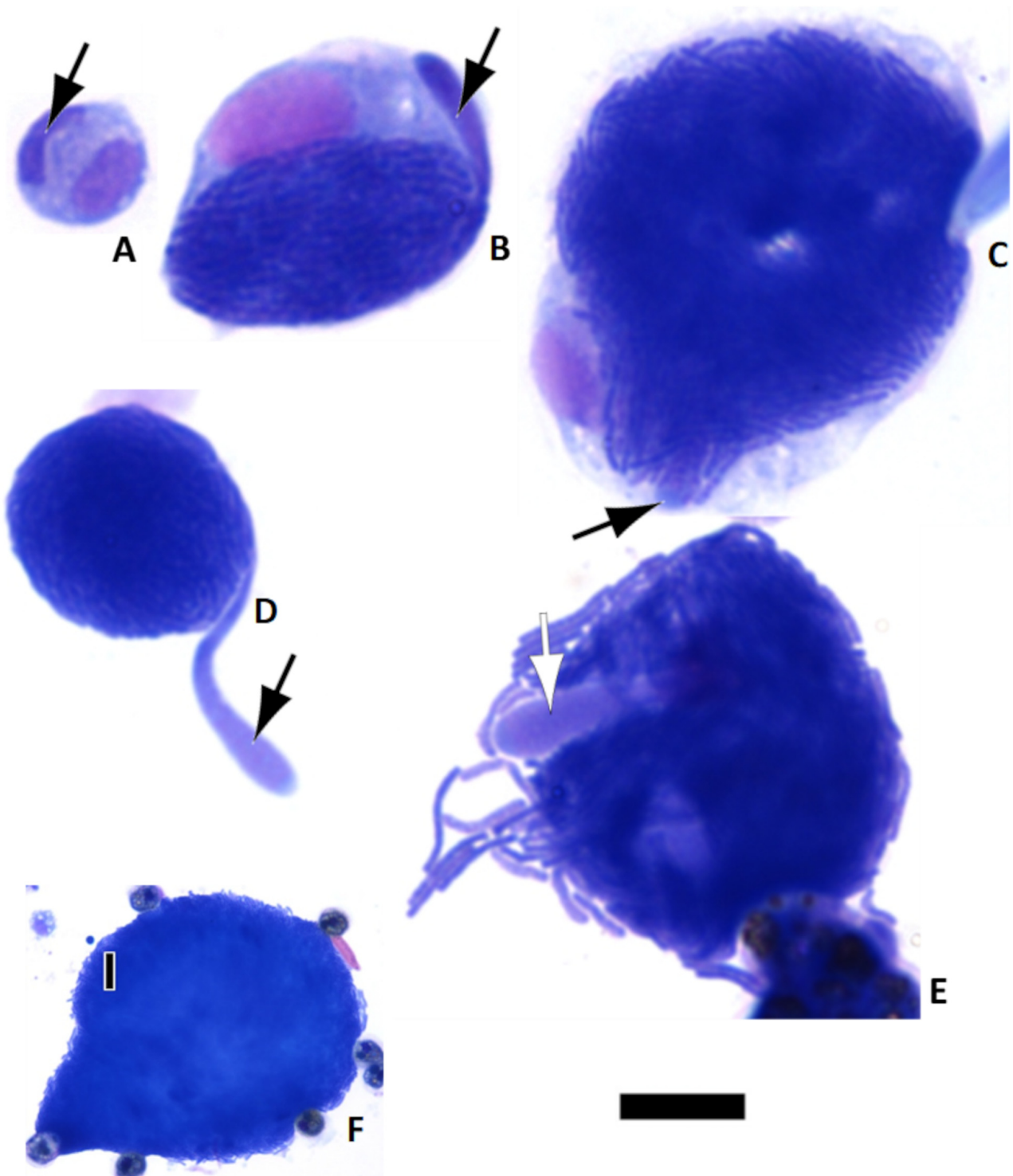


Fig. 5. Intra- and extracellular cell-associated microbial aggregates from apparently healthy *Exaiptasia pulchella* stained with HEMA-3. All images scaled to bar on lower right except for (F) with superimposed vertical scale bar; both bars = 10 μ m. (A) Presumed early stage; note intracytoplasmic basophilic rods (arrow). (B) Presumed medium stage; note clusters of basophilic rods with prominent club-like structure (arrow). (C) Presumed mature stage; note cytoplasm replete with basophilic rods mostly obscuring club-like structure (arrow); pale blue structure to right is portion of adjacent nematocyst. (D) Extracellular cluster of bacteria with club-like structure (arrow). (E) Extracellular cluster of bacteria with bacteria dissociating into individual cells; note club-like structure (arrow). (F) Large extracellular cluster of bacteria with scattered dissociating cells on lower edge

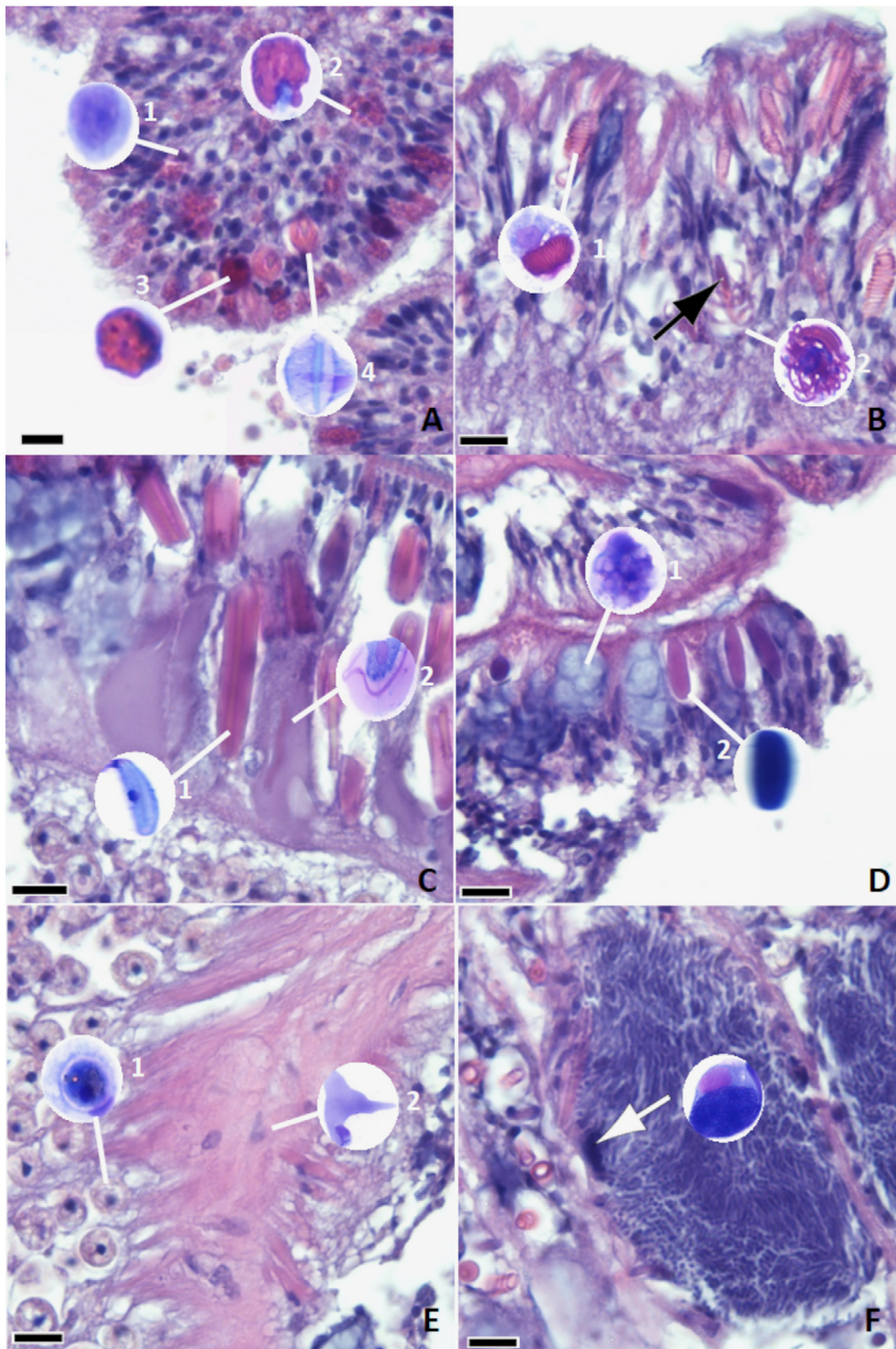


Fig. 6. Photomicrographs of hematoxylin-eosin (HE) stained sections of apparently healthy *Exaiptasia pulchella* along with numbered inserts of light micrographs of corresponding cytology for mesenterial filaments and tentacles. All scale bars = 10 μ m. (A) Mesenterial filament composed of (1) interstitial cells (Fig. 4B, single cell) interspersed with (2) Type 3 granule cell (Fig. 3G, single cell), (3) Type 4 granule cell (Fig. 3H, single cell), and (4) Type 2 cnidocyte (Fig. 1F, single cell). (B) Tentacle epidermis; (1) spirocyte near epidermal surface (Fig. 2J, single cell) and (2) Type 4 cnidocyte (Fig. 2C, single cell) underlying spirocytes; note club-like structure (arrow). (C) Mesenterial filament nematocyst battery; note (1) Type 1 cnidocyte (Fig. 1C, single cell) and (2) larger Type 3 cnidocytes (Fig. 1M, single cell). (D) Mesenterial filament; note (1) mucocytes (Fig. 3K, single cell) and (2) nematocyst (Fig. 1A, single cell). (E) Tentacle; note (1) endosymbionts in gastrodermis adjacent to myoneme (Fig. 4F single cell) with (2) myocyte nuclei (Fig. 4L, single cell). (F) Tentacle epidermis; note cell-associated microbial aggregate replete with basophilic rods and arrow pointing to apparent cross section of club-like structure (Fig. 5B, single cell)

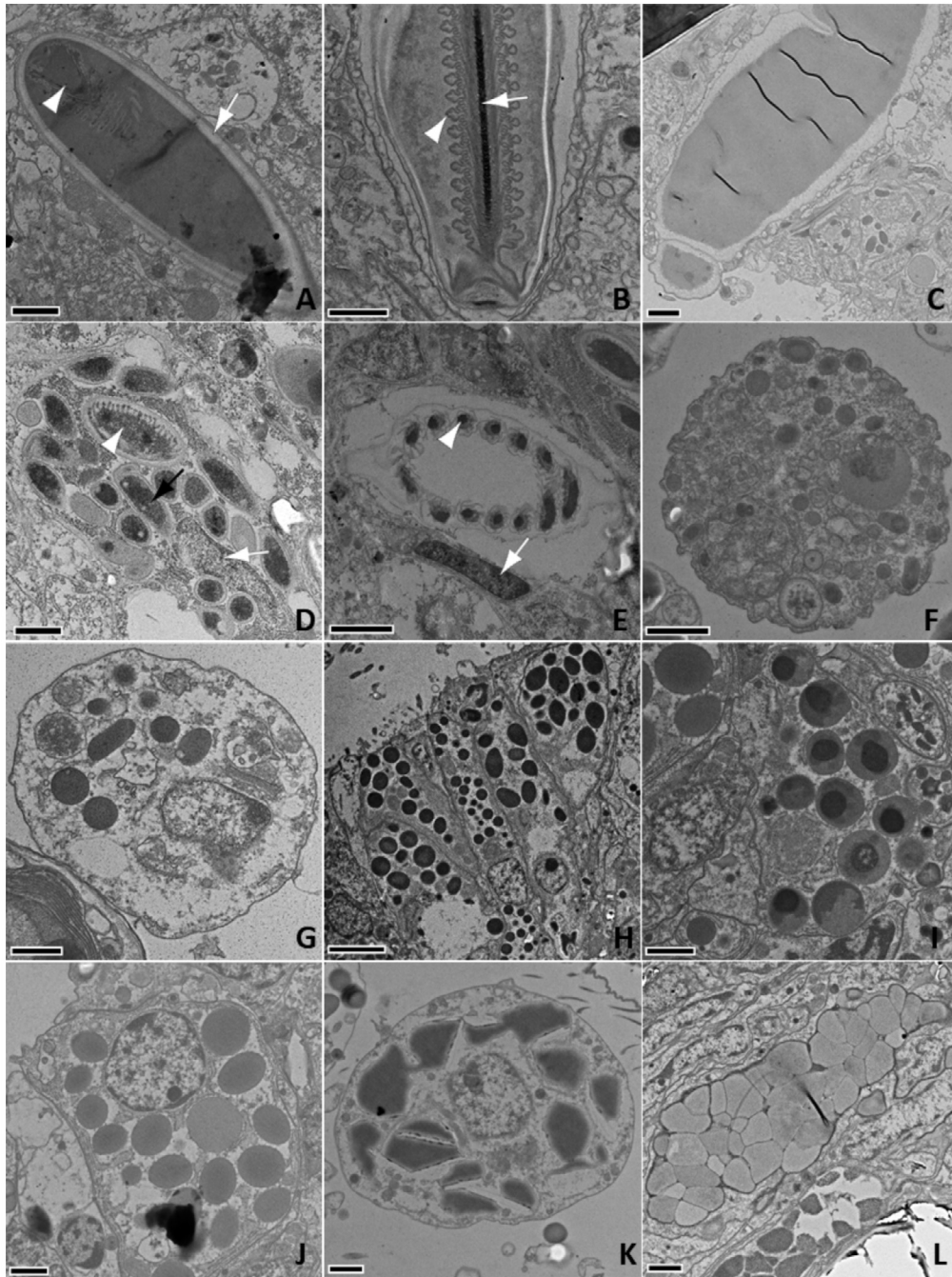


Fig. 7. Transmission electron micrographs of cnidocytes and granule cells of apparently healthy *Exaiptasia pulchella*. (A) Nematocyst (cf. Fig. 1A, light microscopy [LM]); note lanceolate electron-dense matrix with thick capsule (arrow) and filaments (arrowhead). (B) Type 1 cnidocyte (analogue to macrobasic mastigophore) (Fig. 1C,D, LM); note electron-dense central shaft (arrow) surrounded by ornate trichae (arrowhead). (C) Presumed Type 3 cnidocyte (Fig. 1H–N, LM). Note homogeneous electron-dense matrix and thick capsule or large cell. (D) Type 4 cnidocyte (Fig. 2A–E, LM). Note nucleus (white arrow) and club-like structure with ornate internal filaments (arrowhead) surrounded by densely packed atrichous filaments (black arrow). (E) Spirocyte (Fig. 2F–J, LM). Note host cell nucleus (arrow) and electron lucent capsule housing annular arrangement of trichous filaments (arrowhead). (F) Presumed Type 1 granule cell (Fig. 3A–D, LM). Note numerous small round intracytoplasmic granules. (G) Presumed Type 2 granule cell (Fig. 3E,F, LM). Note sparse, large, round, electron-dense granule. (H) Presumed Type 3 granule cell (Fig. 3G, LM). Note closely backed electron-dense granules. (I) Type 4 granule cell (Fig. 3H, LM); note smaller size and closely packed granules with electron-dense core. (J) Type 5 granule cell (Fig. 3I, LM). Note distinct round granules with somewhat lighter color than other granule cells. (K) Presumed Type 6 granule cell (Fig. 3J, LM). Note angular to coarse electron-dense granules. (L) Mucocyte (Fig. 3M, LM). Note indistinct to coalescing, variably sized granules separated by thin membranes. Scale bars = (A,B,D,F,G,I–L) 1 μ m, (C,E) 2 μ m, (H) 4 μ m

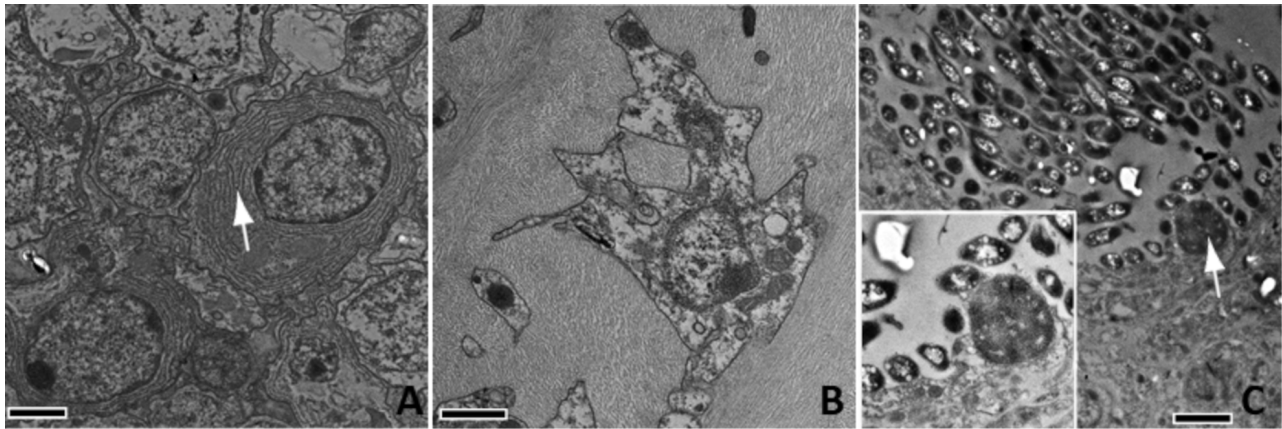


Fig. 8. Transmission electron micrographs of interstitial cells, myocytes, and cell-associated microbial aggregates of apparently healthy *Exaiptasia pulchella*. (A) Interstitial cells (cf. Fig. 4A–E, LM); note variety of morphologies with some cells having prominent rough endoplasmic reticulum (arrow); bar = 1 μ m. (B) Myocyte (Fig. 4J–L, LM) within mesoglea; note angular cell membrane; bar = 0.8 μ m. (C) Bacterial aggregate with club-like structure (arrow) with bar = 2 μ m. Inset shows close up of bacteria and club-like structure

TEM), Type 3 (Fig. 3G, LM; Fig. 7H, TEM), Type 4 (Fig. 3H, LM; Fig. 7I, TEM), Type 5 (Fig. 3I, LM; Fig. 7J, TEM), and Type 6 granule cells (Fig. 3J, LM; Fig. 7K, TEM) were putatively identified based solely on granule densities and morphology that most closely matched that seen on LM. Mucocytes (Fig. 3K–O, LM) had cytoplasm distended by material of moderate electron-density separated by trabeculae of membranes of variable thickness (Fig. 7L, TEM). Interstitial cells (Fig. 4A–E, LM) had a large central nucleus with at times abundant rough endoplasmic reticulum (Fig. 8A, TEM). Myocyte-like cells (Fig. 4J–L, LM) were embedded in mesoglea with sharply angular cytoplasm and prominent mitochondria (Fig. 8B, TEM). Bacterial aggregates (Fig. 5, LM) were populated by elongate to oblong membrane-bound structures enclosing electron-dense reticulated cores (chromatin) containing variably sized round cavities (Fig. 8C, TEM) and a single larger form (Fig. 8C inset).

4. DISCUSSION

The number of cell types identifiable in an organism depends on methods of isolation and examination. Over 40 cell types were identified by single-cell RNA-Seq in *Stylophora pistillata* (Levy et al. 2021). Using acid/glycerin dissociation of cells in *Hydra* and bright-field microscopy of unstained cells, David (1973) identified epithelial, gland, mucous, interstitial, nematoblast, and nerve cells. In unspecified cnidaria, Hündgen (1984) found epitheliomuscular, epidermal,

mucous, ganglion, neurosecretory, neurosensory, general sense, specialized sense, and interstitial cells. It is unclear whether any of the cnidarian cells we saw were neuronal; however, the use of antibodies specific to neuronal type cells on cytological preparations (Wharton et al. 1998) could help clarify neural cells assuming that such antibodies recognize cnidarian epitopes. Pigment cells seen here are probably similar to the melanin-containing cells reviewed by Palmer & Traylor-Knowles (2018). Future studies to sort this could use special stains targeting melanin, such as Fontana Masson (Luna 1968); however, the scarcity of this cell type in our specimens would make this challenging. We identified at least 6 types of granule cells in *Exaiptasia*, but given the limited number of studies using methods outlined here, comparisons with granule cells seen in other studies is difficult. Granular cells have been well documented in cnidaria (Palmer & Traylor-Knowles 2018), particularly in corals and gorgonians, although the role of such cells in cnidarian health or physiology is uncertain (Hawthorn et al. 2023). Possibly, the cells we classified as interstitial cells were akin to agranular, amoebocytes, or hyaline cells reviewed by Palmer & Traylor-Knowles (2018) or interstitial cells in hydra reported by David (1973). Isolating these cells and developing cell-specific markers might help to clarify cell types in cnidaria.

Evidently, *Exaiptasia* cells phagocytize other eukaryotic cells above and beyond endosymbionts, and this phenomenon was seen in Type 1 granule cells, interstitial cells, and Type 4 cnidocytes. Phagocytosis (or possibly emperipolesis) has been documented in the phylum Cnidaria. Olano & Bigger (2000) showed

light micrographs of dissociated cells of the gorgonian *Swifta exserta* phagocytizing India ink. Hutton & Smith (1996) claimed that cells of *Actinia aequina* phagocytized bacteria, whilst Rosental et al. (2017) used FACS 2D plots to show phagocytosis of beads by cells of *Exaiptasia pallida*; however, neither study showed photomicrographs of phagocytizing cells. Snyder et al. (2021) showed that in *Nematostella vectensis* and *Pocillopora damicornis*, phagocytosis of labeled beads, bacteria, and heat-damaged cnidarian cells was dependent on intact cytoskeletal function. Cell-in-cell interactions such as seen here have also been seen in other invertebrates such as sea urchins, and the different types of such interactions are summarized by Work et al. (2020). In that study, it was clear that urchin cells were being phagocytized. In the case of cell-in-cell interactions in *Exaiptasia*, the cells being phagocytized could not be identified and could be food material or housekeeping of damaged host cells as shown by Snyder et al. (2021) for *Pocillopora* or *Nematostella*. For example, Larkman (1984) showed electron micrographs of granule cells of the anemone *Actinia fragacea* phagocytizing particulate matter. We think it unlikely that phagocytized cells were endosymbionts because they did not match the morphology of stained isolated endosymbionts, and they lacked a pyrenoid.

Cytology of *Exaiptasia* suggests that their cnidome might be more complex than what is currently known. *Exaiptasia diaphana* have 3 types of nematocysts: microbasic p-mastigophore (analogous to Type 1 cnidocytes), basitrichous isorhiza (analogous to Type 2 cnidocytes), and spirocytes which dominate (Gundlach & Watson 2019). Schlesinger et al. (2009) used a combination of wet mounts of tissues stained with toluidine blue and histology to reveal the piercing mechanisms of microbasic p-mastigophores (equivalent to Type 1 cnidocytes) in *E. diaphana*. Here, we were able to differentiate at least 3 other types of cnidocytes including Types 2–4 cnidocytes, references to which we were unable to find in the literature. Interestingly, the Type 4 cnidocytes were among the most numerous, at least as enumerated based on methods used here. We concluded these cell types to be some sort of cnidocyte in part due to presence of a central filament (Mariscal 1974) with acidophilic staining properties, a feature of cnidocytes (Cutress 1955). The latter characteristic and the absence of hairs on discharged filaments suggests Type 4 cnidocytes to be some sort of spirocyte distinguished from those cells by a large cell size, coarse filament with a distinct club-like structure on one end. Interestingly, Type 4 cnidocytes seem capable of phagocytosis (Fig. 4P). The closest analogy

we could find were multicellular structures largely comprised of cnidocytes called nematosomes in *Nematostella vectensis* that have a subset of cells able to phagocytize bacteria and labeled beads (Babonis et al. 2016). Spirocytes were similar in morphology on TEM as those described by others (Westfall et al. 1998, 1999). Other features of spirocytes revealed by cytology included the folding of the filaments in some cells (Fig. 2I). Trichae on TEM of Type 1 cnidocytes were similar to fibers seen by Blake et al. (1988).

Cell-associated microbial aggregates in *Aiptasia* have been documented by light and electron microscopy since the late 1980s (McKinstry et al. 1989, Palincsar et al. 1989) and are also seen in corals by histology (Peters et al. 1983, Work & Aeby 2014), and fluorescent *in situ* hybridization (Ainsworth et al. 2006). Like others (McKinstry et al. 1989, Palincsar et al. 1989), we found bacterial aggregates limited to tentacular epidermis. Here cytology provides additional new details not readily seen by the microscopy methods mentioned previously. Specifically, evidence that these clusters are indeed intracellular now seems incontrovertible (Fig. 5A–C). The presence of a club-like structure in both intra- and extracellular forms of these clusters is intriguing and merits further explanation. The ability of these clusters to maintain coherent structure outside the host cells suggests they may not be obligate intracellular organisms. The role of such clusters in cnidarian health remains open to question. In recent studies, bacteria in such clusters have been identified as *Endozoicomonas* sp. in *Stylophora pistillata* (Bayer et al. 2013); however, the morphology of aggregates seen here differs from those of *Endozoicomonas* that are short rods in corals (Chiou et al. 2023). Bacterial endosymbionts have been best studied in arthropods where specialized cells called bacteriocytes house symbiotic bacteria that provide specific nutrients to the insect host (Braendle et al. 2003, Ribeiro Lopes et al. 2021). Insect systems could serve as useful models to evaluate the role of these clusters in cnidarian health.

In summary, we show a method to evaluate cnidarian cells that, although used in *Exaiptasia*, could likely be equally applicable to other cnidaria such as gorgonians or scleractinian corals. We acknowledge that the methods described here such as dissociation of cells with CMFSW and fixation in formalin are unconventional. Typically, cytology is done by daubing tissue blocks on slides, and formalin fixation is generally frowned upon as it might introduce artifacts such as shrinkage and acid hematin precipitation (Satturwar et al. 2020). We found that for *Exaiptasia*,

directly daubing tissues on slides led to sparse cellularity and unsatisfactory morphology with smearing of nuclei and indistinct cells. To improve cell morphology and density in *Exaiptasia*, we opted for formalin fixation and concentrations using a syringe barrel apparatus, in part because we had encountered similar problems of poor cellularity and morphology with cytology of freshly prepared sea urchin coelomocytes that were resolved with the methods used here (Work et al. 2020). We tried CMFSW to dissociate cells, because this solution has prevented reaggregation of sponge cells in experimental settings (Moscona 1963). Whilst formalin fixation might lead to some cell shrinkage (Satturwar et al. 2020), the resulting cellular details as evidenced in the figures seen here seemed to compensate for any shrinkage artifact that might have occurred. Other potential artifacts we might have expected, such as presence of salt crystals due to high salinity of CMFSW, were not seen here. The cell dissociation was not perfect, and tissue clumps and discharged nematocysts were seen in the suspension, but we focused on isolated cells to describe morphology. Because of imperfect dissociation, using this method to quantify cell types would, at best, only provide a crude estimate of relative numbers (see the Appendix). Our methods for processing and staining can result in certain artifacts. For instance, in vertebrates, rapid aqueous Romanowsky (AR) stains such HEMA-3 can result in reduced staining of granules in cytotoxic lymphocytes, mast cells, and basophils, whilst exposure to formalin can lead to excessively blue haze in the cell preparation (Fisher & Meyer 2010). Future studies comparing AR with methanolic stains with and without formalin fixation might help identify whether such artifacts exist for cnidarian cells. However, the poor morphology we observed in unfixed cells might make such comparisons difficult. Formalin fixation prior to staining also enhanced morphologic details in sea urchin coelomocytes (Work et al. 2020) suggesting that staining behavior and artifacts may have some commonalities in invertebrate cells. In the preparations seen here, many cells were round. Yet on histology, epidermal cells are columnar, gastrodermal cells are cuboidal, and calicodermis cells are squamous (Hawthorn et al. 2023); perhaps some of the granular or interstitial cells belonged to some of these layers but cells become rounded following dissociation. On the other hand, in contrast to histology, cytology allowed us to see details such as intracellular microbial aggregates, cnidocyte nematocyst morphology, and cell-in-cell interactions that are not evident histologically. Indeed, cnidocytes comprised a significant percent of

cells seen, and these might have diagnostic value in cnidaria. For example, corals undergoing predation increased density of cnidocytes in tissues (Gochfeld 2004). Cytology might aid in better characterizing such host responses by allowing more refined partitioning of cnidocyte type. Cytology might also reveal developmental processes of cell types, at least based on variation in cell sizes observed, thereby providing a contrast to trying to sort out development of cnidocytes through electron micrographs alone, a challenge recognized by others (Westfall 1966). We have since adapted this method for use in hard corals (*Pocillopora* spp.), and might anticipate using cytology as a complement to histopathology investigations of coral health in the future.

Data availability. Data for this manuscript can be found at: <https://doi.org/10.5066/P9TVTKN9>.

Acknowledgements. Aine Hawthorn and 2 anonymous reviewers provided constructive comments on earlier versions of this manuscript. We thank Norton Chan for access to the Sand Island facility allowing collection of *Exaiptasia*. Any use of trade, firm, or product, names is for descriptive purposes only and does not imply endorsement by the US Government.

LITERATURE CITED

- ✦ Aeby GS, Ushijima B, Campbell JE, Jones S and others (2019) Pathogenesis of a tissue loss disease affecting multiple species of corals along the Florida reef tract. *Front Mar Sci* 6:678
- ✦ Ainsworth TD, Fine M, Blackall LL, Hoegh-Guldberg O (2006) Fluorescence in situ hybridization and spectral imaging of coral-associated bacterial communities. *Appl Environ Microbiol* 72:3016–3020
- ✦ Al-Abbadi MA (2011) Basics of cytology. *Avicenna J Med* 1: 18–28
- ✦ Amodeo AA, Skotheim JM (2016) Cell-size control. *Cold Spring Harb Perspect Biol* 8:a019083
- Arenales A, Almeida ACO, Prado LF, Garcia S, Luvizotto MCR (2014) Cytopathology in the diagnosis of oral trichomoniasis in a rock pigeon (*Columba livia*). *Braz J Vet Pathol* 72:98–99
- ✦ Atkinson CT, Samuel MD (2010) Avian malaria *Plasmodium relictum* in native Hawaiian forest birds: epizootiology and demographic impacts on apapane *Himatione sanguinea*. *J Avian Biol* 41:357–366
- ✦ Babonis LS, Martindale MQ, Ryan JF (2016) Do novel genes drive morphological novelty? An investigation of the nematosomes in the sea anemone *Nematostella vectensis*. *BMC Evol Biol* 16:114
- ✦ Bayer T, Neave MJ, Alsheikh-Hussain A, Aranda M and others (2013) The microbiome of the Red Sea coral *Stylophora pistillata* is dominated by tissue-associated *Endozoicomonas* bacteria. *Appl Environ Microbiol* 79: 4759–4762

- Blake AS, Blanquet RS, Chapman GB (1988) Fibrillar ultrastructure of the capsular wall and intracapsular space in developing nematocysts of *Aiptasia pallida* (Cnidaria: Anthozoa). *Trans Am Microsc Soc* 107:217–231
- Braendle C, Miura T, Bickel R, Shingleton AW, Kambhampati S, Stern DL (2003) Developmental origin and evolution of bacteriocytes in the aphid–*Buchnera* symbiosis. *PLOS Biol* 1:e21
- Camaya AP (2020) Stages of the symbiotic zooxanthellae–host cell division and the dynamic role of coral nucleus in the partitioning process: a novel observation elucidated by electron microscopy. *Coral Reefs* 39:929–938
- Chiou YJ, Chan YF, Yu SP, Lu CY and others (2023) Similar but different: characterization of *dddD* gene-mediated DMSP metabolism among coral-associated *Endozoicomonas*. *Sci Adv* 9:eadk1910
- Cutress CE (1955) An interpretation of the structure and distribution of cnidae in Anthozoa. *Syst Zool* 4:120–137
- David CN (1973) A quantitative method for maceration of hydra tissue. *Wilhelm Roux Arch Entwickl Mech Org* 171:259–268
- Fisher KJ, Meyer DJ (2010) The acquisition and management of cytology specimens. In: Raskin RE, Meyer DJ (eds) *Canine and feline cytology*, 2nd edn. W.B. Saunders, Saint Louis, MO, p 1–14
- Gochfeld DJ (2004) Predation-induced morphological and behavioral defenses in a hard coral: implications for foraging behavior of coral-feeding butterflyfishes. *Mar Ecol Prog Ser* 267:145–158
- Gundlach KA, Watson GM (2019) The effects of symbiotic state and nutrient availability on the cnidom in the model sea anemone, *Exaiptasia diaphana*. *Mar Biol* 166:31
- Hawthorn A, Berzins IK, Dennis MM, Kiupel M and others (2023) An introduction to lesions and histology of scleractinian corals. *Vet Pathol* 60:529–546
- Hündgen M (1984) Cnidaria: cell types. In: Bereiter-Hahn J, Matoltsy AG, Richards KS (eds) *Biology of the invertebrates*. Springer, Berlin, p 45–56
- Hutton DMC, Smith VJ (1996) Antibacterial properties of isolated amoebocytes from the sea anemone *Actinia equina*. *Biol Bull (Woods Hole)* 191:441–451
- Hyman LH (1940) *The invertebrates: Protozoa through Ctenophora*, Vol I. McGraw-Hill, New York, NY
- Kirk AL, Xiang T (2022) Single-cell dissociation of the model cnidarian sea anemone *Exaiptasia diaphana*. *STAR Protoc* 3:101897
- Landsberg JH, Kiryu Y, Peters EC, Wilson PW and others (2020) Stony coral tissue loss disease in Florida is associated with disruption of host–zooxanthellae physiology. *Front Mar Sci* 7:1090
- Larkman AU (1984) The fine structure of granular amoebocytes from the gonads of the sea anemone *Actinia fragacea* (Cnidaria: Anthozoa). *Protoplasma* 122:203–221
- Levy S, Elek A, Grau-Bové X, Menéndez-Bravo S and others (2021) A stony coral cell atlas illuminates the molecular and cellular basis of coral symbiosis, calcification, and immunity. *Cell* 184:2973–2987
- Luna LG (1968) *Manual of histologic staining methods of the Armed Forces Institute of Pathology*, McGraw-Hill, New York, NY
- Mariscal RN (1974) Nematocysts. In: Muscatine L, Lenhoff HM (eds) *Coelenterate biology*. Academic Press, New York, NY, p 129–177
- Martell L, Piraino S, Gravili C, Boero F (2016) Life cycle, morphology and medusa ontogenesis of *Turritopsis dohrnii* (Cnidaria: Hydrozoa). *Ital J Zool* 83:390–399
- McDowell EM, Trump BF (1976) Histological fixatives for diagnostic light and electron microscopy. *Arch Pathol Lab Med* 100:405–414
- McKinstry MJ, Chapman GB, Spoon DM, Peters EC (1989) The occurrence of bacterial colonies in the epidermis of the tentacles of the sea anemone *Aiptasia pallida* (Anthozoa: Actinaria). *Trans Am Microsc Soc* 108:239–244
- Meinkoth JH, Cowell RL (2002) Sample collection and preparation in cytology: increasing diagnostic yield. *Vet Clin North Am Small Anim Pract* 32:1187–1207
- Moscona AA (1963) Studies on cell aggregation: demonstration of materials with selective cell-binding activity. *Proc Natl Acad Sci USA* 49:742–747
- Olano CT, Bigger CH (2000) Phagocytic activities of the gorgonian coral *Swiftia exserta*. *J Invertebr Pathol* 76:176–184
- Palincsar EE, Jones WR, Palincsar JS, Glogowski MA, Mastro JL (1989) Bacterial aggregates within the epidermis of the sea anemone *Aiptasia pallida*. *Biol Bull (Woods Hole)* 177:130–140
- Palmer CV, Traylor-Knowles NG (2018) Cnidaria: anthozoans in the hot seat. In: Cooper EL (ed) *Advances in comparative immunology*. Springer International Publishing, Cham, p 51–93
- Peters EC, Oprandy JJ, Yevich PP (1983) Possible causal agent of 'white band disease' in Caribbean acroporid corals. *J Invertebr Pathol* 41:394–396
- Precht WF, Gintert BE, Robbart ML, Fura R, van Woesik R (2016) Unprecedented disease-related coral mortality in southeastern Florida. *Sci Rep* 6:31374
- Ribeiro Lopes M, Simonet P, Duport G, Gaget K and others (2021) Isolation of insect bacteriocytes as a platform for transcriptomic analyses. *Methods Mol Biol* 2170:185–198
- Romanowsky DL (1890) On the question of the structure of malaria parasites. *Vruch* 11:1171–1173
- Rosental B, Kozhekbaeva Z, Fernhoff N, Tsai JM, Traylor-Knowles N (2017) Coral cell separation and isolation by fluorescence-activated cell sorting (FACS). *BMC Cell Biol* 18:30
- Satturwar S, Rekhman N, Lin O, Pantanowitz L (2020) An update on touch preparations of small biopsies. *J Am Soc Cytopathol* 9:322–331
- Schlesinger A, Zlotkin E, Kramarsky-Winter E, Loya Y (2009) Cnidarian internal stinging mechanism. *Proc R Soc B* 276:1063–1067
- Snyder GA, Eliachar S, Connelly MT, Talice S and others (2021) Functional characterization of Hexacorallia phagocytic cells. *Front Immunol* 12:662803
- Traylor-Knowles N, Baker AC, Beavers KM, Garg N and others (2022) Advances in coral immunity 'omics in response to disease outbreaks. *Front Mar Sci* 9:952199
- Ushijima B, Meyer JL, Thompson S, Pitts K and others (2020) Disease diagnostics and potential coinfections by *Vibrio coralliilyticus* during an ongoing coral disease outbreak in Florida. *Front Microbiol* 11:569354
- Weill R (1934) Contribution a l'étude des cnidaires et de leurs nématocystes. *Trav St Zool Wimereux* 10-11: 1–700
- Weis VM, Davy SK, Hoegh-Guldberg O, Rodriguez-Lanetty M, Pringle JR (2008) Cell biology in model systems as the key to understanding corals. *Trends Ecol Evol* 23:369–376
- Westfall JA (1966) The differentiation of nematocysts and

associated structures in the cnidaria. *Z Zellforsch Mikrosk Anat* 75:381–403

- ✦ Westfall JA, Landers DD, McCallum JD (1998) Different nematocytes have different synapses in the sea anemone *Aiptasia pallida* (Cnidaria, Anthozoa). *J Morphol* 238: 53–62
- ✦ Westfall JA, Landers DD, McCallum JD (1999) Ultrastructure of neuro-spirocyte synapses in the sea anemone *Aiptasia pallida* (Cnidaria, Anthozoa, Zoantharia). *J Morphol* 241: 165–173
- ✦ Wharton SB, Chan KK, Hamilton FA, Anderson JR (1998) Expression of neuronal markers in oligodendrogliomas: an immunohistochemical study. *Neuropathol Appl Neurobiol* 24:302–308
- Work TM (2023) Coral reef ecosystem health. In: Jessup DA, Radcliffe RW (eds) *Wildlife disease and health in conser-*

vation. Johns Hopkins University Press, Baltimore, MD, p 7–21

- ✦ Work TM, Aeby GS (2014) Microbial aggregates within tissues infect a diversity of corals throughout the Indo-Pacific. *Mar Ecol Prog Ser* 500:1–9
- ✦ Work T, Meteyer C (2014) To understand coral disease, look at coral cells. *EcoHealth* 11:610–618
- ✦ Work TM, Millard E, Mariani DB, Weatherby TM and others (2020) Cytology reveals diverse cell morphotypes and cell-in-cell interactions in normal collector sea urchins *Tripneustes gratilla*. *Dis Aquat Org* 142:63–73
- ✦ Work TM, Weatherby TM, Landsberg JH, Kiryu Y, Cook SM, Peters EC (2021) Viral-like particles are associated with endosymbiont pathology in Florida corals affected by stony coral tissue loss disease. *Front Mar Sci* 8: 750658

Appendix

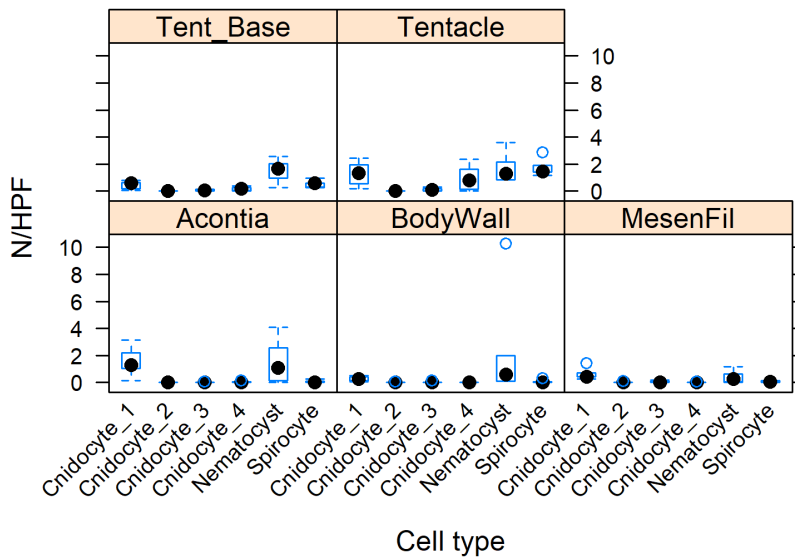


Fig. A1. Counts per 100× microscope field (HPF; field of view = 0.2) of 6 cnidocyte types or nematocysts from 6 *Exaiptasia pulchella* partitioned by tentacle base, tentacle, acontia, body wall, and mesenterial filaments. Black dot is median, boxes are the interquartile range, whiskers are 1.5× interquartile range, and points are outliers

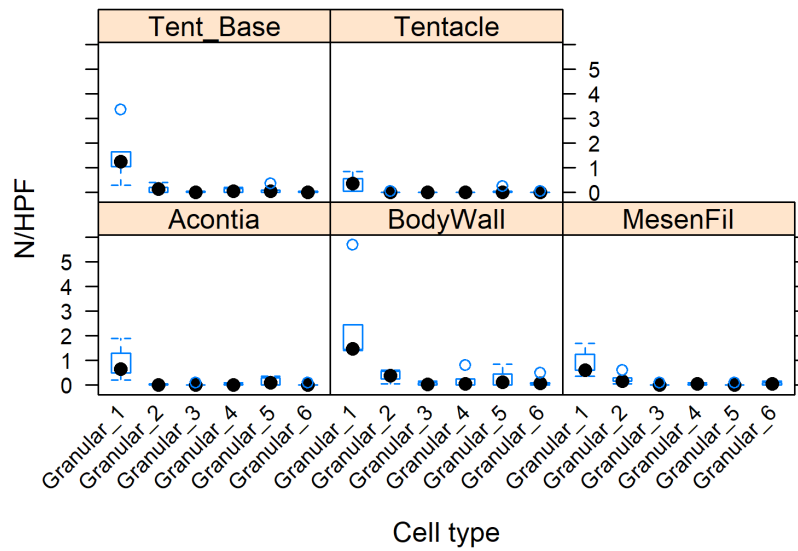


Fig. A2. Counts per 100× microscope field (field of view = 0.2) of 6 granule cell types from 6 *Exaiptasia pulchella* partitioned by tentacle base, tentacle, acontia, body wall, and mesenterial filaments. Box plot parameters as in Fig. A1

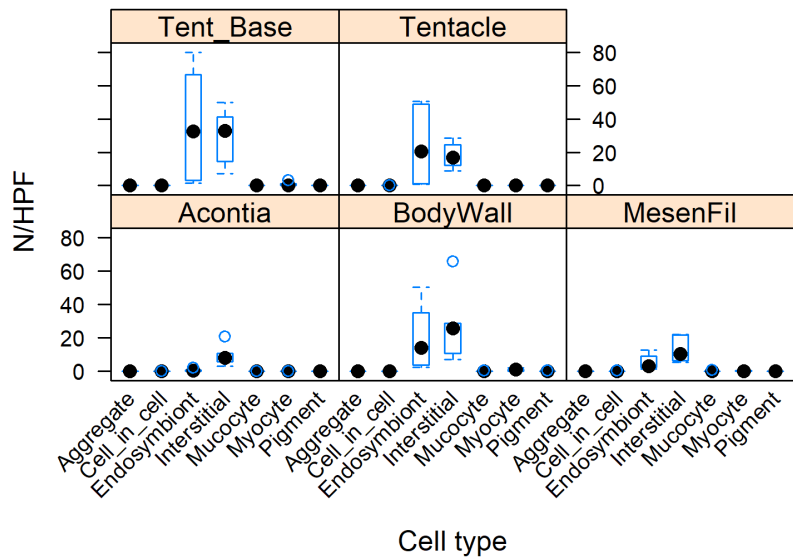


Fig. A3. Counts per 100× microscope field (field of view = 0.2) of other cell types from 6 *Exaiptasia pulchella* partitioned by tentacle base, tentacle, acontia, body wall, and mesenterial filaments. Box plot parameters as in Fig. A1

Editorial responsibility: Esther C. Peters,
Fairfax, Virginia, USA
Reviewed by: J. Arnold and M. Dennis

Submitted: September 14, 2023
Accepted: February 16, 2024
Proofs received from author(s): April 10, 2024